

## Detecting chaos in particle accelerators through the frequency map analysis method

Yannis Papaphilippou<sup>1, a)</sup>

*European Organisation of Nuclear Research - CERN, Geneva,  
Switzerland*

(Dated: 9 June 2014)

The motion of beams in particle accelerators is dominated by a plethora of non-linear effects which can enhance chaotic motion and limit their performance. The application of advanced non-linear dynamics methods for detecting and correcting these effects and thereby increasing the region of beam stability plays an essential role during the accelerator design phase but also their operation. After describing the nature of non-linear effects and their impact on performance parameters of different particle accelerator categories, the theory of non-linear particle motion is outlined. The recent developments on the methods employed for the analysis of chaotic beam motion are detailed. In particular, the ability of the frequency map analysis method to detect chaotic motion and guide the correction of non-linear effects is demonstrated in particle tracking simulations but also experimental data.

PACS numbers: Valid PACS appear here

---

<sup>a)</sup>Electronic mail: Ioannis.Papaphilippou@cern.ch

Due to their collective nature and the external electro-magnetic fields employed for guiding and focusing them, the dynamics of beams in particle accelerators is intrinsically non-linear. The performance of a wide spectrum of accelerators, ranging from ultra-high energy hadron colliders with several kilometres of circumference to X-ray storage rings and high-power synchrotrons, can be severely limited by the resulting chaotic motion, impacting the machine availability but also construction and operating cost. Methods based on high order perturbation theory have found ample room for application in beam dynamics. A breakthrough in the field was the introduction of the Frequency Map Analysis method<sup>42-44</sup> which enables the analysis of multi-dimensional Hamiltonian systems and the clear distinction between ordered and chaotic trajectories, which are either computed by direct numerical integration or experimentally measured in operating accelerators. This paper reviews the modern trends in detecting chaos in particle accelerators giving emphasis to the application of frequency map analysis in a variety of beam dynamics problems.

---

## I. INTRODUCTION

The last few years were remarkable for CERN and the scientific community of particle physics with the discovery of the Higgs boson by the two experiments ATLAS<sup>1</sup> and CMS<sup>16</sup>, which culminated with the attribution of the 2013 Nobel prize in physics to Fran cois Englert and Peter Higgs<sup>54</sup>. These outstanding experimental results were also due to the excellent performance of the Large Hadron Collider (LHC), a superb scientific instrument for particle physics research.

Modern accelerator rings as the LHC are pushing their design and operating parameters into regimes of extreme beam currents and small phase space beam volumes (the so called emittance), the ratio of which roughly represents the beam brightness, a measure of accelerator performance. In these high-brightness regimes, non-linear effects become predominant and the motion of particles at large amplitudes becomes chaotic. This can lead to physical increase of the beam size and to particle losses, which do not only affect performance but can also be harmful for machine equipments and reduce the accelerator availability. The

application of advanced non-linear dynamics methods during the design but also operation of accelerators is thus important for studying and ensuring the long-term stability of particle motion. These studies have to guide the design of accelerator components providing tolerances for the quality of magnetic fields, their alignment, the stability of the power supplies, the use of corrector magnets adequately grouped for the alleviation of these effects, and all these, at the smallest possible cost.

In this paper, we review the basics of non-linear beam dynamics in particle accelerator rings, the effects that are responsible for the onset of chaos, the methods used for detecting this chaotic motion and how these methods guide accelerator design for increasing the beam stability. Particular emphasis is given to the Frequency Map Analysis (FMA)<sup>42–44</sup>, which has been proven a very robust numerical method for exploring and understanding the global dynamics of any non-linear Hamiltonian system.

The paper is organised as follows: in section II, the fundamentals of non-linear particle beam motion are briefly recalled, including the accelerator Hamiltonian, one-turn maps and normal forms. The next section is devoted to the review of different chaos detection techniques in beam dynamics and in particular the FMA method. The application of this method in various accelerator rings and non-linear beam dynamics problems is presented in section IV. Experimental non-linear dynamics techniques are elaborated in section V before closing with the summary.

## II. NON-LINEAR BEAM DYNAMICS BASICS

### A. The accelerator Hamiltonian

In any circular accelerator, particles are moving inside vacuum pipes under the influence of self-generated but also external three-dimensional electromagnetic fields. Electric fields produced by radio-frequency (RF) cavities are usually used to accelerate particles and affect mostly longitudinal (“synchrotron”) motion, whereas magnetic fields are used for their guidance and dominate transverse (“betatron”) motion. Self-fields are represented by Coulomb forces within the particles of the same beam or through image charges in the vacuum chamber or between two closely interacting beams and dominate collective beam motion.

Neglecting self fields and radiation, the system can be described by a single-particle Hamiltonian<sup>36</sup>

$$H(\mathbf{x}, \mathbf{p}, t) = c\sqrt{\left(\mathbf{p} - \frac{e}{c}\mathbf{A}(\mathbf{x}, t)\right)^2 + m^2c^2} + e\Phi(\mathbf{x}, t) \quad , \quad (1)$$

where  $\mathbf{x} = (x, y, z)$  are the usual Cartesian positions,  $\mathbf{p} = (p_x, p_y, p_z)$  their conjugate momenta,  $\mathbf{A} = (A_x, A_y, A_z)$  the magnetic vector potential,  $\Phi$  the electric scalar potential,  $m$  the particles rest mass,  $c$  the speed of light and  $e$  the electric charge. Using Hamilton's equations  $(\dot{\mathbf{x}}, \dot{\mathbf{p}}) = [(\mathbf{x}, \mathbf{p}), H]$ , the usual Lorentz equations for charged particle motion in electromagnetic fields can be obtained.

The Hamiltonian represents a time-dependent three degrees of freedom system. It is useful (especially for rings) to transform the Cartesian coordinate system to the Frenet-Serret system moving to a closed curve, with path length  $s$  and make a further canonical transformation that uses this path length as the independent variable instead of the time  $t$ .

The longitudinal motion can be approximated by a time-dependent (periodic) pendulum and is generally slow, with frequencies of the order of a few KHz. On the other hand, transverse motion is dominated by the magnetic vector potential of each individual magnet represented by homogeneous polynomials. This motion is generally much faster with frequencies of the order of a few MHz. Hence, the two motions can be decoupled, at first approximation (e.g. the electric field component can be ignored). In addition, the magnetic fields can be considered static within a magnet and transverse to particle motion, so that the magnetic vector potential has only one component, the longitudinal one. Following Maxwell equations and the theory of analytic functions, it can be shown that the vector potential component for a certain magnet becomes<sup>67</sup>

$$A_z(x, y) = -B_0r_0\Re e \sum_{n=0}^{\infty} \frac{b_n(s) - ia_n(s)}{n+1} \left(\frac{x+iy}{r_0}\right)^{n+1} \quad , \quad (2)$$

where  $r_0$  is the reference radius which is chosen to be the outermost conceivable deviation of the particles and  $B_0$  the main field of the magnet. The coefficients  $b_n(s)$  and  $a_n(s)$  are named the normal and skew multipoles, due to the associated magnetic field symmetry imposed by the homogeneous polynomials. In this convention, the dipole terms are represented for  $n = 0$ , the quadrupole for  $n = 1$ , the sextupole for  $n = 2$ , the octupole for  $n = 3$ , etc.

Taking into account that the total momentum is much larger than the transverse (generally true for high energy accelerators), the square root of the Hamiltonian (1) can be expanded to leading order. Following some further approximations for large rings (imposing

$x \ll \rho$ ) and applying additional canonical transformations, by rescaling the transverse momenta to the reference one and moving the periodic orbit to the origin<sup>68</sup>, the Hamiltonian takes the form

$$\mathcal{H} = \frac{p_x^2 + p_y^2}{2(1 + \delta)} - \frac{x(1 + \delta)}{\rho(s)} - e\hat{A}_s \quad , \quad (3)$$

where  $\delta = \frac{P_t - P_0}{P_0}$  is the relative momentum deviation of the particles' momentum  $P_t$  with respect to the reference momentum of the accelerator  $P_0$  and  $\rho$  the radius of curvature of the reference orbit. This  $s$ -dependent Hamiltonian has now 2 degrees of freedom plus the path length  $s$  and for a ring it is periodic with period the circumference.

The Hamiltonian then can be written in a more suitable form for dynamical analysis, by separating it to an integrable part and a non-integrable one:

$$\mathcal{H}' = \mathcal{H}_0 + \sum_{k_x, k_y} h_{k_x, k_y}(s) x^{k_x} y^{k_y} \quad , \quad (4)$$

where  $h_{k_x, k_y}(s)$  are associated with the multipole coefficients and thereby are also periodic. The integrable Hamiltonian is derived by considering only dipole (uniform) fields with radius of curvature  $\rho(s)$  and normal quadrupole (linear) magnetic fields, with normalised gradient  $K(s)$ :

$$\mathcal{H}_0 = \frac{p_x^2 + p_y^2}{2(1 + \delta)} - \frac{x\delta}{\rho(s)} + \frac{x^2}{2\rho(s)^2} + \frac{K(s)}{2}(x^2 - y^2) \quad . \quad (5)$$

The equations of motion are Hills equations (harmonic oscillators with periodic coefficients) and can be solved following Floquet theory<sup>22</sup>. For analysing the non-integrable part, classical perturbation theory was employed already in the early days of the first synchrotrons 32-34,52,72.

## B. Accelerator maps and normal forms

Classical perturbation theory permits the estimation of the "resonance driving terms", the Fourier amplitudes associated to a particular resonance, issued by an expansion of the periodic perturbation of the Hamiltonian, in a Fourier series. In principle, the technique works for arbitrary order in the Taylor expansion of the perturbation, but the disentangling of variables becomes difficult even to 2nd order. This can be solved by the introduction of the Lie formalism, where the application of perturbation theory becomes completely algorithmic. In addition, the same formalism can be used for building and analysing a

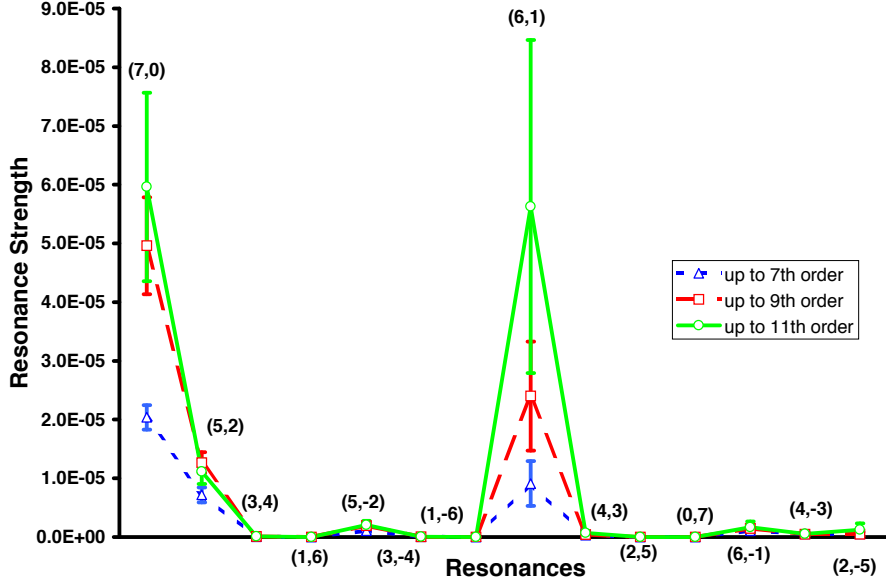


FIG. 1. Average value (circles) and standard deviation (error bars) of the 7th order resonance strengths, computed at an amplitude close to the minimum chaotic boundary, over 60 random realisations of the multipole errors of an LHC magnet model. The three different curves represent resonance driving terms estimated by taking into account three different orders of the generating function produced by a normal form analysis of a numerical one-turn map<sup>61</sup>.

symplectic accelerator map<sup>23–25,27</sup>. This becomes even more appealing in the case of the accelerator rings, made out of thousands of elements.

For a general Hamiltonian system  $H(\mathbf{z}, t)$ , the Hamiltons equations  $\frac{d\mathbf{z}}{dt} = [H, \mathbf{z}] =: H : \mathbf{z}$  are represented by the usual Poisson bracket operator  $: f : g = [f, g] = \sum_{i=1}^N \left( \frac{\partial f}{\partial p_i} \frac{\partial g}{\partial q_i} - \frac{\partial f}{\partial q_i} \frac{\partial g}{\partial p_i} \right)$ . A formal solution is written as

$$\mathbf{z}(t) = \sum_{k=0}^{\infty} \frac{t^k : H :^k}{k!} \mathbf{z}_0 = e^{t:H} : \mathbf{z}_0 , \quad (6)$$

with  $\mathcal{M} = e^{t:H}$  a symplectic map in its usual exponential Lie operator representation. The one-turn accelerator map is a polynomial of degree  $m$  in the conjugate variables  $z_1, \dots, z_n$ , represented by the composition of the maps

$$\mathcal{M} = e^{:f_2:} e^{:f_3:} e^{:f_4:} \dots ,$$

where the generators  $f_i$  are related to the Hamiltonians for each element. Differential algebra tools can be used for computing efficiently the map<sup>12</sup>. The construction of normal forms on

the map consists of finding a symplectic transformation which so that it becomes simpler. The generating function of this transformation can be represented by a polynomial in the new variables, whose coefficients represent the "strength" of various resonances of the accelerator. The numerical application of these technique in the numerical map enable the evaluation of resonance strengths and can be used for dictating correction schemes<sup>9,28</sup>. An example of this normal form analysis for the LHC is shown in Fig. 1, where a numerical tool was built in order to evaluate and represent graphically resonance strengths up to any order<sup>61</sup>. In this plot, the 7th order resonance strengths are depicted, issued by a normal form analysis of a numerically constructed 11th order map, for a given amplitude, close to the minimum chaotic boundary of this LHC model. The points correspond to the average value of the resonance driving terms over the 60 random realisations of the magnet errors and the error bars are equal to one standard deviation. The three different lines represent 7th order resonance strengths the computation of which is conducted up to three different orders in the generating function of the map (7th, 9th and 11th). With this method, the predominance of the (7,0) and (6,1) resonances was revealed including the important contribution of the higher orders in the generating function, for accurately computing the resonance strengths. Although it was thought that the dynamics of the LHC at injection is largely determined by the random multi-pole errors in the super-conducting dipoles, which fill a large part of the ring, the method enabled to discover the importance of a few warm quadrupoles<sup>61</sup>.

### III. CHAOS DETECTION METHODS - THE FREQUENCY MAP ANALYSIS

The accelerator Hamiltonian (4) is not bounded, so particles inside the chaotic regions of the system will diffuse to infinity, or in a real accelerator will be lost in the vacuum pipe. The focus of non-linear beam dynamics is to estimate and take correcting measures in order to increase the area in real space where particles survive after some time, the so-called dynamic aperture (DA). This quantity (or particle survival rates) can be measured in a real accelerator<sup>13,15,78</sup>, or calculated through numerical integration of the equations of motions (called particle tracking), with codes optimised for this task<sup>69,70</sup>. This brute-force approach, although providing a clear measure of accelerator performance, presents clear drawbacks. Firstly, the simulation has to be carried out for very large rings with thousands

of elements and for particles which need to survive several millions (or practically infinite number) of turns. This can be numerically heavy and it has to be repeated for several random realisations of the magnetic errors, in order to provide some statistical confidence about the robustness of the results. This can be partially solved by detecting the chaotic behaviour of the trajectory with some fast indicators such as the Lyapunov exponents<sup>31,71</sup>, the variance of unperturbed action<sup>18,35,75</sup> or Fokker-Planck-like diffusion coefficients<sup>14,73</sup>. On the other hand, none of these approaches can solve the more serious problem which is the need of understanding globally the systems phase space structure.

The aforementioned high-order perturbation theory has been extensively used in beam physics in order to provide insight regarding the non-linear dynamics of particle beams. However, it is not easy to correlate the computed resonance driving terms with the extent of the chaotic region, or to put it simply, which are the resonances that limit the DA in order to provide correcting measures.

A method that bridges this gap and can be used both as an early chaos indicator but also for numerically estimating resonance strengths, through tracking or measured data, is the Frequency Map Analysis (FMA). This method has been extensively used in celestial mechanics<sup>39,40,47</sup>, galactic dynamics<sup>59,60</sup>, atomic physics<sup>51</sup> Hamiltonian toy models<sup>26,41,45</sup> and became a standard tool of beam dynamics analysis for a variety of accelerators, such as hadron colliders<sup>50,55,56,63,64</sup>, synchrotron light sources<sup>46,53,58,62,65</sup>, high-intensity rings<sup>7,57</sup>, B-factories<sup>48</sup> and linear collider damping rings<sup>2</sup>. The method relies on the high precision calculation<sup>42</sup> of the associated frequencies of motion (or "tunes" in the accelerator jargon), which are supposed to be invariant in the case of quasi-periodic motion, as stated by the KAM theory. In this respect, the variation of the frequencies over time<sup>26,41,55</sup> can provide an excellent early stability indicator that has the advantage of connecting resonant structure with diffusion of chaotic trajectories.

The first step is to derive through the Numerical Analysis of Fundamental Frequencies (NAFF) algorithm<sup>39,40</sup> or variants of this code<sup>6</sup>, a quasi-periodic approximation, truncated to order  $N$ ,

$$f'_j(t) = \sum_{k=1}^N a_{j,k} e^{i\omega_{jk}t}, \quad (7)$$

with  $f'_j(t), a_{j,k} \in \mathbb{C}$  and  $j = 1, \dots, n$ , of a complex function  $f_j(t) = q_j(t) + ip_j(t)$ , formed by a pair of conjugate variables of a general  $n$ -degrees of freedom Hamiltonian system, which are



determined by usual numerical integration or experimentally measured, for a finite time span  $t = \tau$ . The next step is to retain from the quasi-periodic approximation the fundamental frequencies of motion, corresponding most of the times to the frequency of the dominant Fourier component  $\omega_{j1}$ , for each degree of freedom. In this respect, the frequency vector  $\frac{\omega}{2\pi} = \boldsymbol{\nu} = (\nu_1, \nu_2, \dots, \nu_n)$  can be constructed, which, up to numerical accuracy<sup>42</sup>, parameterizes the KAM tori in the stable regions of a non-degenerate Hamiltonian system. Then, the construction of the frequency map can take place<sup>26,41,45,46</sup>, by repeating the procedure for a set of initial conditions which are transversal to the orbits of interest. As an example, we may keep all the momenta  $\mathbf{p}$  constant, and explore the positions  $\mathbf{q}$  to produce the map  $\mathcal{F}_\tau$ :

$$\mathcal{F}_\tau : \begin{array}{l} \mathbb{R}^n \longrightarrow \mathbb{R}^n \\ \mathbf{q}|_{\mathbf{p}=\mathbf{p}_0} \longrightarrow \boldsymbol{\nu} . \end{array} \quad (8)$$

The dynamics of the system is then analysed by studying the regularity of this map on frequency or initial condition space. In addition, each initial condition can be associated with a diffusion indicator, by computing the frequency vector for two equal and successive time spans, which correspond to half of the total integration time  $\tau$ . The amplitude of the diffusion vector,

$$\mathbf{D}|_{t=\tau} = \boldsymbol{\nu}|_{t \in (0, \tau/2]} - \boldsymbol{\nu}|_{t \in (\tau/2, \tau]} , \quad (9)$$

can be used for characterising the instability of each orbit. Through this representation the traces of the resonances can be viewed in the physical space, as well, and set a threshold for the minimum DA. Moreover, a diffusion quality factor defined as the average of the local diffusion coefficient to the initial amplitude of each orbit, over a domain  $R$  of the phase space:

$$D_{QF} = \left\langle \frac{|\mathbf{D}|}{|\mathbf{q}_0|} \right\rangle_R . \quad (10)$$

This quantity can be used for the comparison of different designs and the optimisation of the correction schemes proposed.

## IV. APPLICATION OF FREQUENCY MAP ANALYSIS IN ACCELERATOR MODELS

### A. Frequency maps for the LHC

The long term stability of the beam is the major concern for the design of a hadron collider, as the LHC. Especially during long injection period of more than  $10^7$  turns needed to fill the LHC with more than 2800 bunches per beam, in its nominal configuration, particle trajectories are perturbed strongly by non-linear magnet fields, mainly attributed to the multipole errors of the super-conducting magnets. In order to reach the target DA of 12 rms

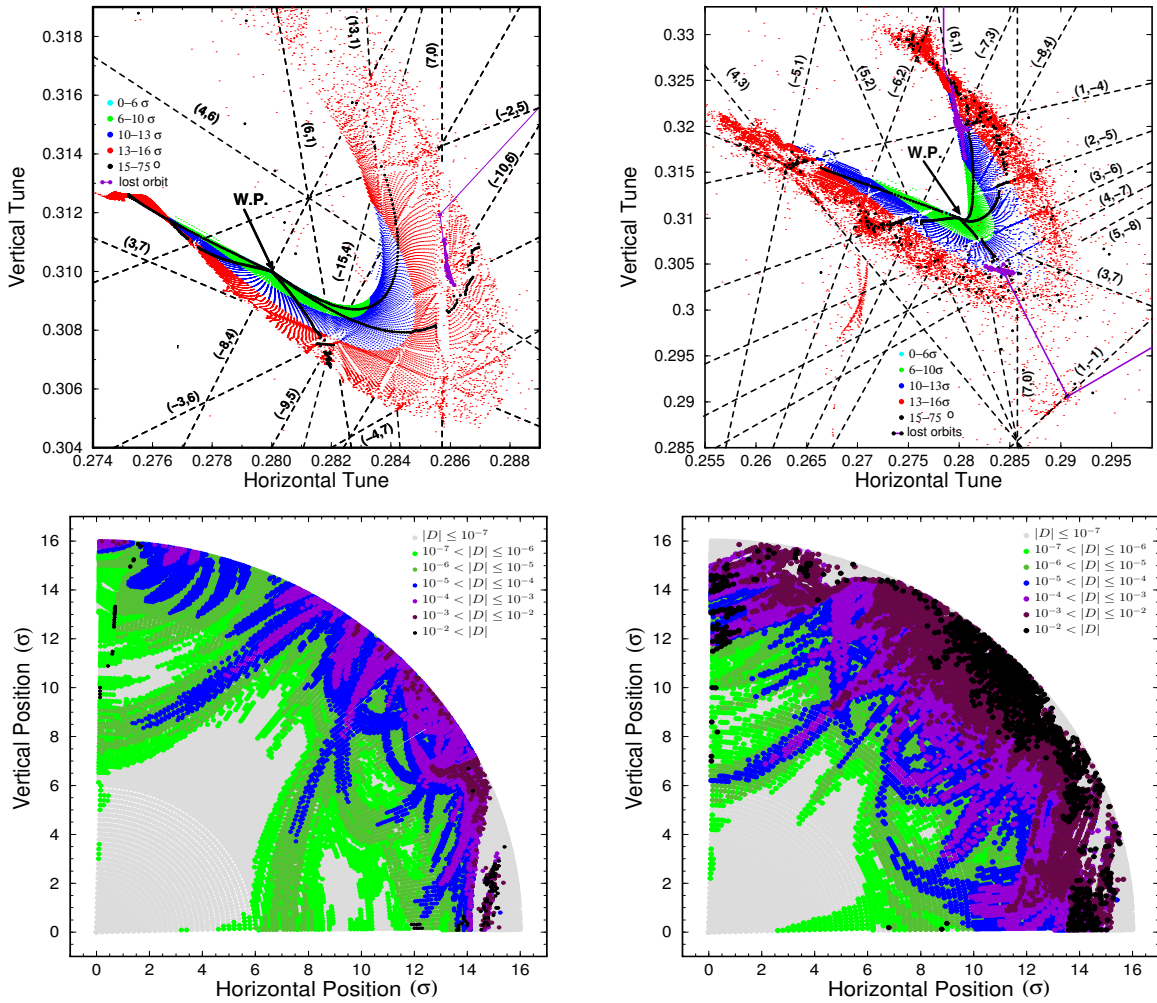


FIG. 2. Frequency (top) and diffusion (bottom) maps for the LHC target error table without (left) and with (right) the high  $a_4$  value on the dipoles.<sup>55</sup>

beam sizes  $\sigma_x = \sigma_y = \sigma$ , for the LHC injection optics, giving a necessary safety factor of 2 with respect to the physical aperture restriction of the beam at  $6\sigma$  (location of collimators protecting the super-conducting magnets), a target magnetic multi-pole error table was proposed. A frequency map for this error table and for the nominal tunes ( $Q_x = 64.28$ ,  $Q_y = 59.31$ ) is shown in the top left part of Fig. 2<sup>55</sup>. This specific machine gives an average DA of around  $13\sigma$  and a minimum of  $12\sigma$ , values which are close to the average and minimum DA over all the 60 random realisation of the magnet errors. Each point in the frequency space corresponds to a particular on-momentum orbit tracked over 1000 turns. The different colours in the map correspond to orbits with different initial position amplitudes (from  $0-16\sigma$ ) and the black dots label initial conditions with different amplitude ratios (from  $15^\circ$  to  $75^\circ$ ). The orderly spaced points correspond to regular orbits whereas the dispersed points to chaotic ones. This plot is a snapshot of the so called Arnold web<sup>3</sup>, the network of resonances  $a\nu_x + b\nu_y + c = 0$ , which appear as distortions of the map (empty and filled lines) and can be easily identified. For example, the importance of three 7th order resonances ( $(a, b) = (7, 0), (6, -1)$  and  $(-2, 5)$ ) is put in evidence. Especially the crossings of the resonant lines are “hot spots”, from which particles can easily diffuse: as an example, the evolution of the frequency vector of an orbit starting close to the crossing of the  $(7, 0)$  with the  $(-3, 6)$  and  $(4, 6)$  resonances is shown (purple dots). The orbit diffuses along the unstable manifold of the 7th order resonance and is lost after a few thousand turns. This is a clear demonstration of the importance of this resonance with respect to the DA of this model.

One of the main issues in the specification of the LHC injection optics, is the correction of the systematic part of the lowest order multipole errors of the super-conducting dipoles, which limit the DA<sup>38</sup>. This is usually done by magnetic coils (“spool pieces”) placed at the ends of the dipoles. In the case of more realistic error table with increased normal and skew octupoles, there was an important loss of the DA<sup>37</sup> with respect to the target error table. A frequency map for the same random “seed” as for the previous case with the increased skew octupole error in the dipoles is shown in the top right plot of Fig. 2. The frequency maps now looks much more distorted. The most remarkable feature concerning the system’s dynamics is the huge increase of the tune variation with amplitude, to the point that particles are diffusing towards the  $(1, -1)$ -resonance, in the right bottom corner of the map. On the other hand, particles close to horizontal motion at the top of the map

are approaching the  $(0, 3)$  resonance and the ones close to vertical motion the  $(4, 0)$ . This finding has been confirmed with Normal Form analysis<sup>37</sup>. The dynamic aperture could be recovered by tuning the skew octupole spool pieces such as to cancel the  $(1, -1)$  resonance<sup>37</sup>.

The global dynamics of these two cases can be also explored in the physical space of the system by mapping each initial condition with the diffusion vector (9), the amplitude of which can be used for characterising the instability of each orbit. In Figs. 2 (bottom), the points in the configuration space are plotted using a different colour coding corresponding to different diffusion indicators in logarithmic scale: from grey for stable ( $|\mathbf{D}| \leq 10^{-7}$ ) to black for strongly chaotic particles ( $|\mathbf{D}| > 10^{-2}$ ), that actually are lost within that short integration time. Through this representation, the traces of the resonances in the physical space are clearly visible, and thereby a threshold for the minimum DA can be set.

The diffusion quality factor (10) is a very efficient global chaos indicator for comparing different designs and optimising the correction schemes proposed<sup>7,56,74</sup>. For example, for the normal octupole  $b_4$  and decapole  $b_5$  correctors in the LHC, five schemes were proposed, regarding the positioning and the amount of the correctors<sup>56</sup>. Frequency maps were produced for all the correction cases and two working points. In Fig. 3, the diffusion quality factor averaged over the angles is plotted in logarithmic scale versus the amplitude, for both working points, for all correction schemes and for the non-zero momentum deviation. These plots confirmed that all the correction schemes are quite similar and indeed necessary, following the comparison with the diffusion quality factor with no correction (black dots). They also indicated that the nominal (but most expensive) solution of including correctors in all the super-conducting dipole (blue dots) was not performing better than the one with correctors in every second dipole (red dots), which actually presented a slightly better diffusion quality factor. Based on this study, the baseline correction for the LHC was to have correctors in every second dipole, which was also a cost effective solution. Finally, this study demonstrated that the diffusion quality factor is correlated with other global chaos indicators, such as the resonances driving terms norm and the dynamic aperture<sup>56</sup>.

## B. Working point choice through frequency maps

Frequency map analysis is naturally very powerful for choosing the best working point of an accelerator. An example is given in Fig. 4, where the value of the tune diffusion

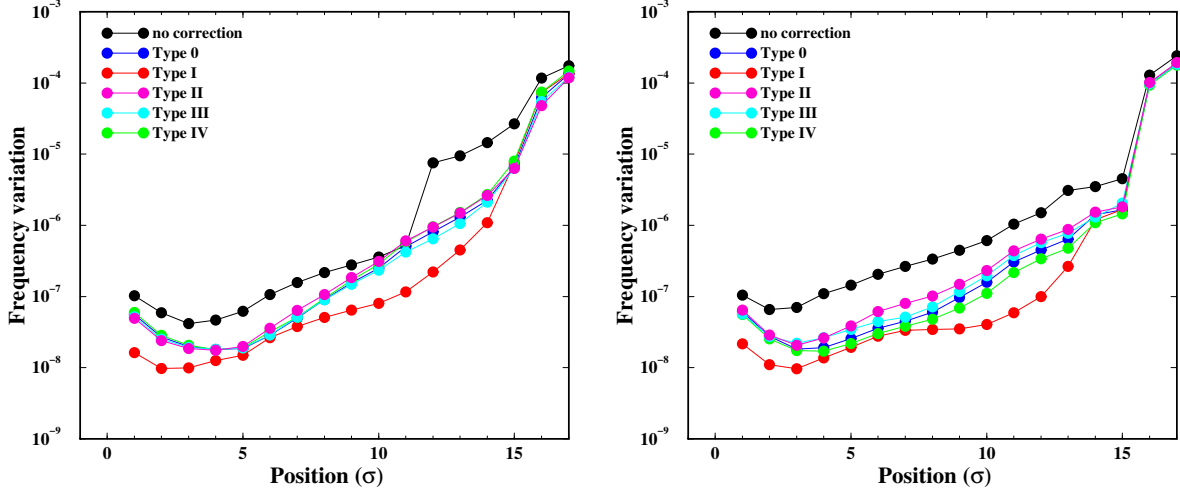


FIG. 3. Evolution of the frequency variation averaged over all directions, with the particles' amplitude (in  $\sigma$ ) for  $\delta p/p = 7 \times 10^{-4}$ , and for two different tunes:  $(Q_x, Q_y) = (0.28, 0.31)$  (left) and  $(Q_x, Q_y) = (0.21, 0.24)$  (right)<sup>56</sup>.

coefficient is plotted versus the momentum deviation  $\delta p/p$ , for all working points of the Spallation Neutron Source accumulator ring<sup>57</sup>, currently in operation in Oak-Ridge National Laboratory and holding the beam power world record. The single-particle dynamics of this ring is dominated by edge effects in the magnets, and especially the quadrupole fringe fields, which are octupole-like<sup>27</sup>. Four working points were selected and compared corresponding to the different curves of Fig. 4. The peak values on the diffusion indicators, for all working points correspond to areas of the phase space that are perturbed due to 4th order resonances, showing the destructive effect of quadrupole fringe fields. The dotted lines on the plots represent the average values of the diffusion indicators for all tracked momentum deviations. It is clear that (6.23,6.20) is the best choice, followed by (6.4,6.3). Their performance can be further improved by using the available multi-pole correctors<sup>57</sup>, for correcting the normal and skew 3rd order resonances, in the case of (6.4,6.3), and the 4th order normal resonances in the case of (6.23,6.20). The other two working points have the disadvantage of crossing major resonances, which are very difficult to correct. Based on this study, the nominal working point of the SNS ring was chosen to be (6.23,6.20) and was successfully used in commissioning and operation until today.

Similar working point optimisation was employed for different type of rings such as SuperB, a lepton collider designed at INFN-LNF<sup>48</sup>, or the PS2 ring<sup>7</sup>, an upgrade project of

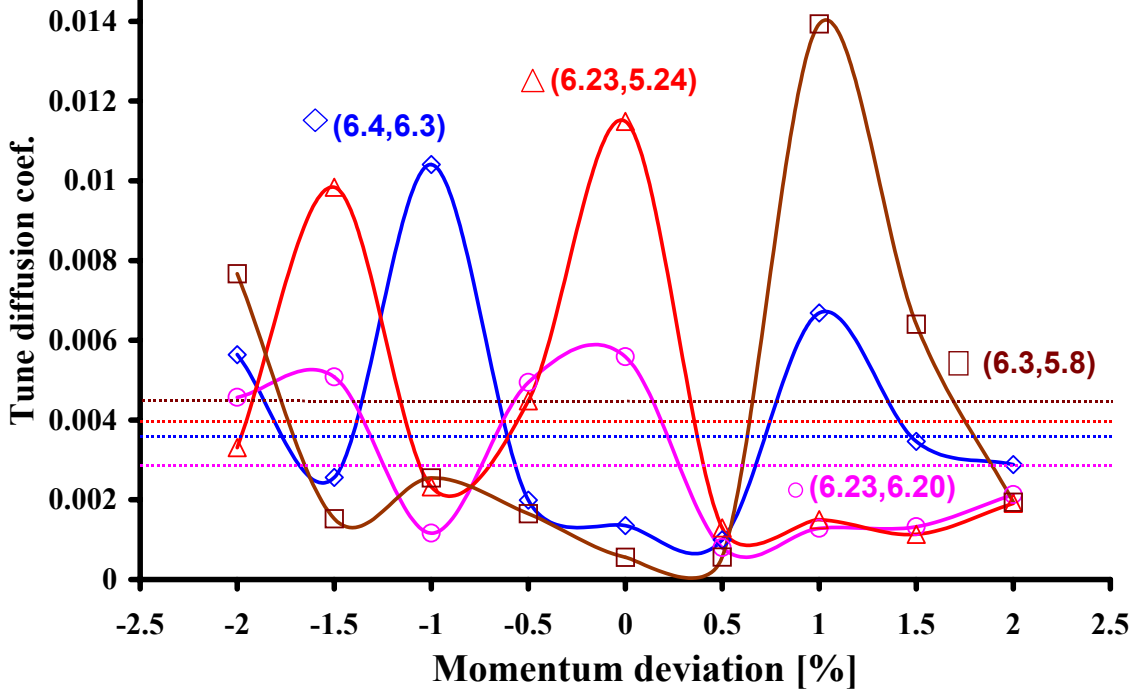


FIG. 4. Tune diffusion coefficients for four SNS working points versus the different momentum deviations.<sup>57</sup>

the current CERN Proton Synchrotron.

### C. Chaotic behaviour due to the long range beam-beam interaction

In a colliding-beam storage ring, one of the largest perturbations affecting the motion of beam particles is the collision with the opposing beam. This interaction occurs, unavoidably, in the form of head-on collisions between bunches of the two beams at designated interaction points. Hadron colliders employ long trains of closely spaced bunches, and individual bunches encounter many others of the opposing beam at various long-range collision points, where the beams are not fully separated into two disjunct beam pipes. In general, the effect of the long-range collisions depends on the ratio of the beam separation to the local rms beam size, and on the total number of long-range collision points. On either side of the two LHC main collision points, a beam encounters about 15 long-range collisions with an approximate average separation between the closed orbits of the two beams of 9.5 rms beam sizes.

Simulations predict that the long-range collisions in hadron colliders give rise to a well defined border of stability<sup>35,63</sup>. Following standard ideas popularised by Chirikov and his

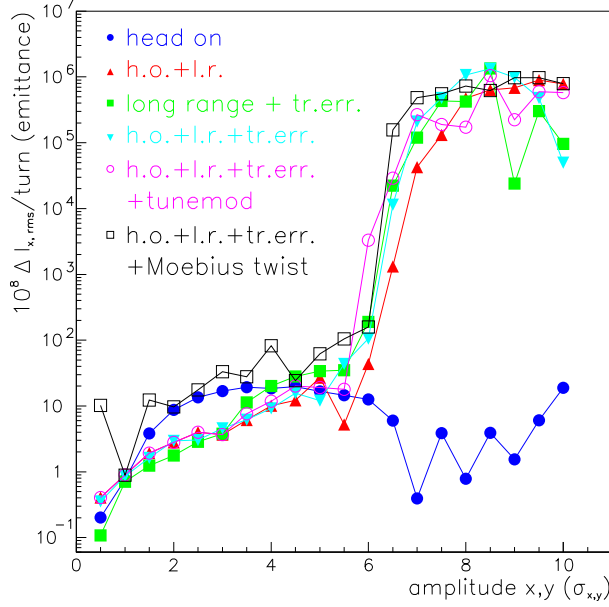


FIG. 5. The change of action variance per turn as a function of the starting amplitude. Compared are the cases: head-on collisions only (dark blue), head-on and long-range collisions (red), long-range collisions plus triplet field errors (green) both types of collisions plus triplet field errors (light blue), the additional effect of a tune modulation at the synchrotron frequency (22 Hz) of amplitude  $10^{-4}$  (pink), the additional effect of a Möbius twist (black)<sup>63</sup>.

collaborators<sup>17,18</sup>, a diffusion coefficient can be estimated by calculating the variance of the unperturbed actions for a large number of turns. Fig. 5 displays the change of the action variance, in terms of beam sizes, as computed by beam-beam simulations which consider the particle motion in a 4-dimensional transverse phase space for a model with 2 interaction points and parameters similar to those of the LHC<sup>63</sup>. The stability border is insensitive to the presence of the head-on collision (filled circles with dark blue curve), and only marginally affected by the nonlinear field errors in the final-triplet quadrupoles (squares with green curve) or by a small additional tune ripple (empty circles with pink curve). This “diffusive aperture” with long-range collisions is equally insensitive to transverse closed-orbit offsets between the two beams at the head-on collision points<sup>63</sup>.

The top part of figure 6 presents frequency maps obtained by tracking single particles over 1000 turns under the influence of beam-beam effects. Red dots represent particles with initial transverse amplitudes up to  $5 \sigma_{x,y}$ , whereas blue dots show results for initial amplitudes up to

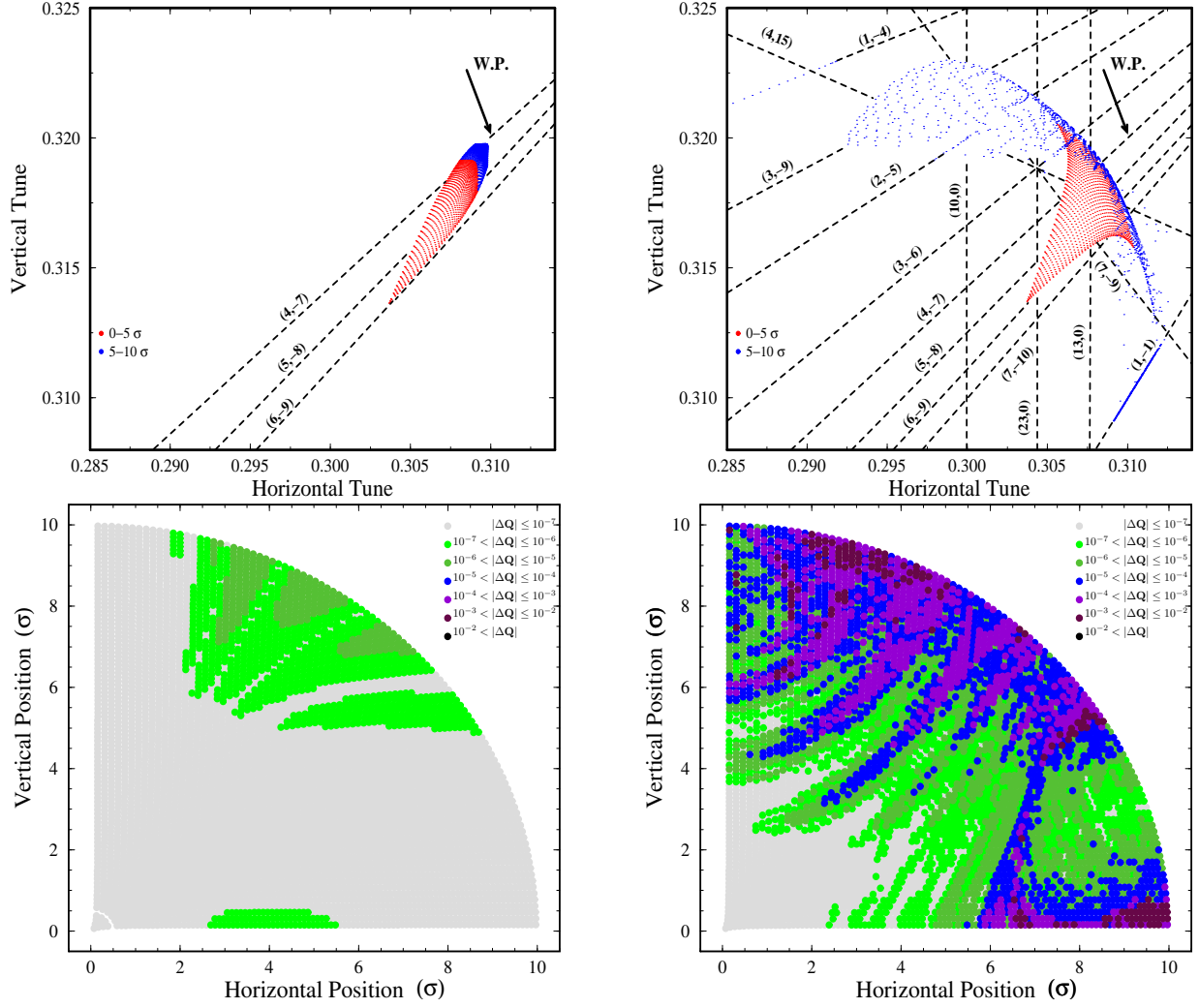


FIG. 6. Frequency (top) and diffusion (bottom) maps for head-on collisions only (left) and including long-range collisions, as well (right)<sup>63</sup>.

$10 \sigma_{x,y}$ . The dramatic effect of the long-range collisions is revealed through the comparison of the maps obtained with (right) and without (left) the long-range effects. Up to initial particle amplitudes of around  $6 \sigma_{x,y}$ , the effect of the head-on collisions dominates. Then, the long-range effect takes over and the frequency map flips, as the tune shift with amplitude changes direction. This non-monotonic dependence of the tune with respect to the amplitude is potentially dangerous for the stability of particles beyond this limit<sup>41,43</sup>. The conclusions of the previous paragraph regarding the dominant destabilising role of the long-range collisions are also confirmed in the diffusion maps at the bottom plots of Fig. 6.

In Fig. 7, the diffusion quality factor versus the amplitude, averaged over all initial am-



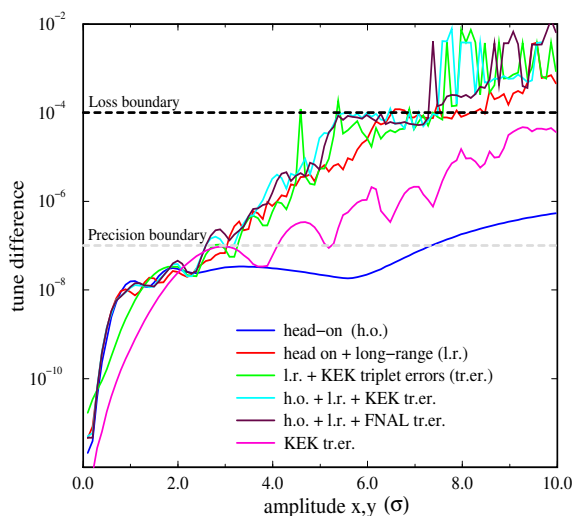


FIG. 7. The change of frequency per 500 turns averaged over all initial amplitude ratios  $x - y$  as a function of the starting amplitude. Compared are the cases: head-on collisions only; head-on and long-range collisions; long-range collisions plus triplet field errors; both types of collisions plus triplet field errors; both types of collisions plus triplet field errors; only triplet errors.

plitude ratios is plotted, for different combinations of beam-beam and triplet nonlinearities (quadrupole magnets focusing the beam at the collision point). There are two thresholds marking the precision boundary and a particle loss boundary for tune changes bigger than  $10^{-4}$ . Considering linear frequency diffusion over time, this corresponds to one unit in frequency within  $10^7$  turns, which certainly induces particle loss. For all the cases where long-range collisions and triplet field errors are included, the loss boundary is located at the same point, around  $5.5\sigma_{x,y}$ . For the case where the triplet field errors are not added to the beam-beam effect, the threshold is reached a little further, around  $6\sigma_{x,y}$ . The case with only triplet errors is clearly more stable, but indeed there is still a visible effect for larger initial amplitudes. No effect whatsoever can be observed for the case with only the head-on effect included, where the tune variation is very close to the precision limit of the method.

## D. Dynamics of the CLIC Pre-damping rings

The main limitation of the DA in the low emittance lattices comes from the non-linear effects induced by the strong sextupole magnet strengths, which are introduced for the correction of the tune change with momentum (chromaticity). Following first order perturbation theory<sup>11</sup>, the strength of a resonance  $n_x Q_x + n_y Q_y = p$  of order  $n$ , with  $|n_x| + |n_y| = n$  the order of the resonance and  $p$  any integer, vanishes within an ensemble of  $N_c$  cells, if the resonance amplification factor is<sup>77</sup>

$$\left| \sum_{p=0}^{N_c-1} e^{ip(n_x \mu_{x,c} + n_y \mu_{y,c})} \right| = \sqrt{\frac{1 - \cos[N_c(n_x \mu_{x,c} + n_y \mu_{y,c})]}{1 - \cos(n_x \mu_{x,c} + n_y \mu_{y,c})}} = 0 \quad , \quad (11)$$

with  $\mu_{x,y}$  the horizontal and vertical phase advance of the cell. Note that the tune is just the total phase advance for one turn. The previous condition is achieved when  $N_c(n_x \mu_{x,c} + n_y \mu_{y,c}) = 2k\pi$ , provided the denominator of Eq. (11) is non zero, i.e.:  $n_x \mu_{x,c} + n_y \mu_{y,c} \neq 2k'\pi$ , with  $k$  and  $k'$  any integers. From this, a part of a circular accelerator will not contribute to the excitation of any non-linear resonances, except of those defined by  $\nu_x \mu_x + \nu_y \mu_y = 2k_3\pi$ , if the phase advances per cell satisfy the conditions:  $N_c \mu_x = 2k_1\pi$  and  $N_c \mu_y = 2k_2\pi$ , where  $k_1$ ,  $k_2$  and  $k_3$  are any integers. Prime numbers for  $N_c$  are interesting, as there are less resonances satisfying both diophantine conditions simultaneously.

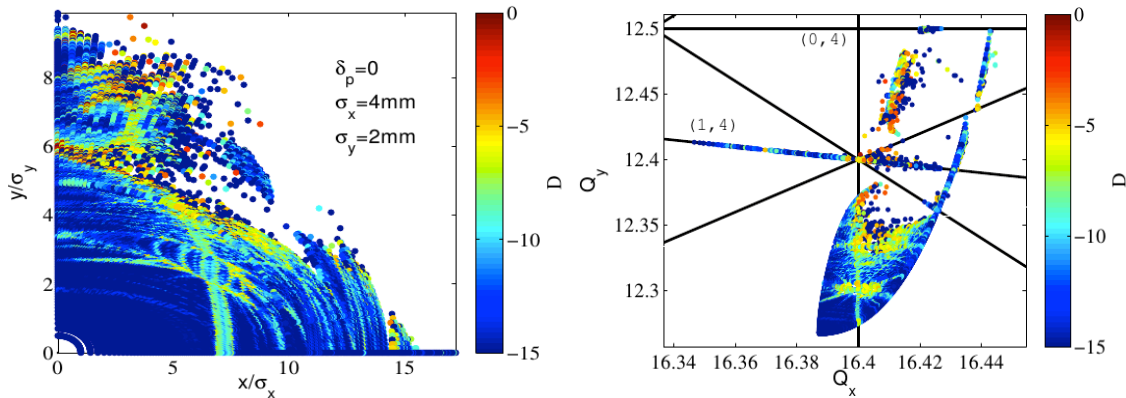


FIG. 8. Frequency maps (right) and diffusion maps (left) for on-momentum particles, in the CLIC PDRs, for the working point  $(16.39, 12.26)^2$ .

The nonlinear optimisation of the pre-damping rings (PDR), in the injector complex of the future Compact Linear Collider (CLIC), was based on this “resonance free lattice

concept”<sup>2</sup>. Tracking of particles with different initial conditions for 1024 turns, was performed with MADX-PTC<sup>70</sup>, for a model of the lattice including sextupoles and fringe fields. Fig. 8 presents frequency and diffusion maps for trajectories that survived over 1024 turns, color-coded with the diffusion coefficient of Eq. (9), for on-momentum particles. From the frequency maps it is observed that the tune is crossing the (1,4) resonance, which is not eliminated by the resonance free lattice and the phase advances chosen ( $\mu_x = 5/17$ ,  $\mu_y = 3/17$ ). This seems to be the main limitation of the DA. The shape of the frequency maps, especially at high amplitudes, does not have the triangular shape expected by the linear dependence of the tune shift to the action, and foldings appear. This occurs when terms of higher order in the Hamiltonian become dominant over the quadratic terms, as the amplitude increases. This behaviour occurs due to the suppression of the lower order resonances, following the resonance free lattice concept.

## V. EXPERIMENTAL NON-LINEAR BEAM DYNAMICS

### A. Experimental frequency analysis

One of the most impressive aspects of frequency analysis is its ability to be directly applied in experimental accelerator data. Early studies<sup>10</sup> have shown that the Fourier amplitudes of experimental turn-by-turn (TBT) position data from an accelerator can be associated to resonance driving terms. In more recent years<sup>4,5,76</sup> and due to the high precision of the NAFF algorithm<sup>39,40</sup>, frequency analysis of experimental data became quite popular for evaluating and correcting non-linear particle beam motion. At the same time, it was possible to construct experimental frequency maps<sup>65</sup>, thereby guiding the experimental calibration of the non-linear accelerator model.

In particular, at the European Synchrotron Radiation Facility (ESRF) storage ring, an experimental frequency map measurement campaign was initiated<sup>58,62</sup>, providing new insight regarding the dynamic aperture limitation of the operational working point. This can be viewed in the left part of Fig. 9, where an experimental frequency map is produced for a large number of horizontal beam excitations and a constant vertical one and the TBT position data are recorded in beam positions monitors (BPM), around the ring. The map can be roughly separated in three regions: For small amplitudes, the frequency dependence

with the amplitude has a regular behaviour. At intermediate amplitudes, there is a zone of instability characterised by the accumulation of points on resonant lines or gaps. Most of the resonances are of the fifth or tenth order. Finally, for bigger amplitudes, the frequency path is regular, crossing a multitude of 8th order resonances that are not excited. The last point, where losses begin to occur, approaches an area of potential instability, the crossing point of all third order resonances and the coupling resonances  $(1, -1)$ . A frequency map resulting from a numerical simulation of a model<sup>58</sup> suggested that the excited zone in the vicinity of the 3rd order resonance is large enough to induce beam loss, as far as the last measured tunes in this experiment. The same resonance was responsible for the radical reduction of the DA for momentum deviation of  $+2.5\%$ <sup>62</sup>.

The right plot of Fig. 9 represents a frequency map with a detuned sextupole correction. High order two dimensional resonances appear to be excited. The frequency space is very distorted, and the dynamic aperture is limited near the area of the 5th order resonance. This shows how the frequency map can be used as a guide to understand the impact of different machine settings in the beam stability.

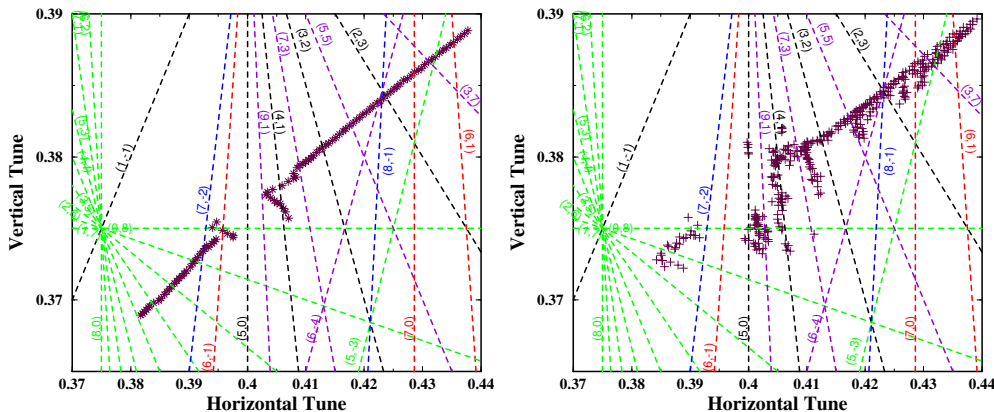


FIG. 9. Frequency map for the ESRF storage ring for the nominal sextupole correction (left) and with a detuned sextupole (right), for the working point  $(36.44, 14.39)$ <sup>62</sup>.

## B. Loss maps in frequency space

Especially in hadron rings, where the frequency variation with amplitude may be quite small, even up to the physical amplitude limitation, dynamic variation of the tunes for measuring particle losses due to resonance crossing is a well established technique since

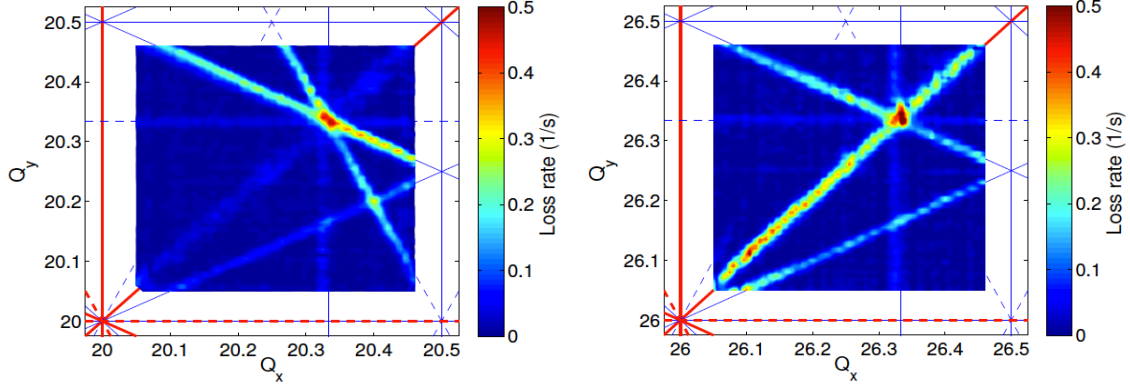


FIG. 10. Experimental tune scans in the SPS with the nominal (Q26) optics (left) and the low  $\gamma_t$  Q20 optics (right). The color-code indicates the loss rate during a dynamic scan of the fractional tunes, as obtained by averaging over 4 scan directions.

decades<sup>19–21,29,30,66</sup>. The measurement principle of the dynamic tune scan used here for comparing resonance behaviour of two optics in the Super Proton Synchrotron (SPS)<sup>8</sup> can be described as follows: the beam intensity is recorded during a slow variation of the betatron tunes. Large particle oscillations are induced when the working point is close to a resonance, which results in particle loss. The strength of the resonances can be inferred from the slope of the recorded losses as function of time. In order to enhance the observed losses and thus increase the sensitivity to resonances, the beam is injected deliberately with a large injection error in both planes for provoking transverse emittance blow-up. The resulting resonance diagrams for two optics are shown in Fig. 10, where the colour code indicates the loss rate, averaged over the four scan directions. Resonances up to third order can be clearly identified in both optics. In the case of Q26 optics (left), it appears that the difference coupling resonance  $Q_x - Q_y$  was creating higher particle losses compared to the Q20 optics (right). The normal sextupole resonances  $3Q_x$ ,  $Q_x - 2Q_y$  and  $Q_x + 2Q_y$  and the skew resonance at  $3Q_y$  seem to be excited in both optics. A surprisingly strong third order skew resonance at  $2Q_x + Q_y$  is observed in the Q20 optics. However, the area close to the fractional tunes usually used for the LHC beams in the SPS (0.13, 0.18) is free of strong resonances in both optics.

## VI. SUMMARY

The study and correction of non-linear effects is crucial for the design and performance optimisation of particle accelerators. Non-linear dynamical system methods are fundamental in order to achieve this task. The application of the frequency map analysis has become a necessary step for understanding and improving the dynamics of accelerator models. Apart from the global viewing of the dynamics in frequency space and the association of resonant lines to configuration space, it can provide a frequency quality factor in order to compare different design and correction approaches. In the case of the LHC, frequency map analysis coupled with normal form construction and dynamic aperture simulations enabled the identification of dangerous high order resonances at injection, guided the choice of correction systems and clearly demonstrated the dominant effect of long range beam-beam interactions, at collision. The method was proven very efficient for choosing the working point of high-power proton rings like the SNS accumulator and guided the design of a low emittance ring such as the CLIC pre-damping rings. The application of the method to experimental data gives great insight regarding the dynamic behaviour of an operating accelerator, such as the ESRF storage ring or the SPS at CERN. Although the method is now well-established for single particle dynamics analysis, it has not yet been applied to study collective particle motion, in a full 6-dimensional, time-varying phase space, with the further inclusion of dissipative effects, due to synchrotron radiation damping. This would be one of the key future challenges which would push the method even beyond its original scope and frame of applicability.

## ACKNOWLEDGEMENTS

I would like to express my gratitude to Jacques Laskar for introducing me to frequency map analysis and the tremendous impact his early mentoring had to the rest of my scientific career. I am indebted to the organisers of the workshop on “Methods of Chaos Detection and Predictability: Theory and Applications” for giving me the opportunity to present this review and in particular to Charis Skokos for his long-time friendship and collaboration. Finally, I would like to acknowledge the contributions of Fanouria Antoniou, Hannes Bartosik, Frank Schmidt and Frank Zimmermann to a number of the presented results.

## REFERENCES

- <sup>1</sup>Aad, G. *et al.* (ATLAS Collaboration), “Observation of a new particle in the search for the Standard Model Higgs boson with the ATLAS detector at the LHC,” *Phys.Lett.* **B716**, 1–29 (2012).
- <sup>2</sup>Antoniou, F. and Papaphilippou, Y., “Analytical considerations for linear and nonlinear optimization of the TME cells. Application to the CLIC pre-damping rings,” *ArXiv e-prints* (2013), accepted for publication in *Physical Review Special Topics - Accelerator and Beams*, arXiv:1310.5024 [physics.acc-ph].
- <sup>3</sup>Arnold, V. I., “Proof of a Theorem by A. N. Kolmogorov on the invariance of quasi-periodic motions under small perturbations of the Hamiltonian,” *Russian Math. Survey* , 13–40 (1963).
- <sup>4</sup>Bartolini, R., Martin, I., Rowland, J., Kuske, P., and Schmidt, F., “Correction of multiple nonlinear resonances in storage rings,” *Phys. Rev. ST Accel. Beams* **11**, 104002 (2008).
- <sup>5</sup>Bartolini, R. and Schmidt, F., “Normal form via tracking or beam data,” *Part. Accel.* **59**, 93–106 (1997).
- <sup>6</sup>Bartolini, R. and Schmidt, F., “SUSSIX: A computer code for frequency analysis of nonlinear betatron motion,” in *Proceedings of the workshop Nonlinear and Stochastic Beam Dynamics in Accelerators : a Challenge to Theoretical and Computational Physics*, CERN-SL-98-17-AP, edited by A. Bazzani, J. Ellison, and H. Mais (DESY, Hamburg, 1998) pp. 390–394.
- <sup>7</sup>Bartosik, H. and Papaphilippou, Y., “Linear and Non-Linear Optimization of the PS2 Negative Momentum Compaction Lattice,” in *Proceedings of the 46th ICFA Advanced Beam Dynamics Workshop on High-Intensity and High-Brightness Hadron Beams, Morschach, Switzerland* (e-proceedings, 2010) pp. 67–71.
- <sup>8</sup>Bartosik, H., Papaphilippou, Y., and Arduini, G., “Optics considerations for lowering transition energy in the SPS,” in *Proceedings of the 2nd International Particle Accelerator Conference 2011, San Sebastián, Spain*, MOPS012, edited by C. Petit-Jean-Genaz (2011) pp. 619–621.
- <sup>9</sup>Bazzani, A., Todesco, E., Turchetti, G., and Servizi, G., *A normal form approach to the theory of nonlinear betatronic motion*, CERN Yellow report (CERN, Geneva, 1994).

- <sup>10</sup>Bengtsson, J., *Non-linear transverse dynamics for storage rings with applications to the low-energy antiproton ring (LEAR) at CERN*, Ph.D. thesis, Lund U., Geneva (1988), presented on 1 Aug 1988.
- <sup>11</sup>Bengtsson, J., “The Sextupole Scheme for the Swiss Light Source: An Analytic Approach,” Tech. Rep. PSI Internal Report SLS-Note 9/97 (PSI, 1997).
- <sup>12</sup>Berz, M., “Differential algebraic description of beam dynamics to very high orders,” Part. Accel. **24**, 109–124 (1989).
- <sup>13</sup>Brüning, O. S., Schmidt, F., Fischer, W., and Willeke, F., “Comparison of measured and computed dynamic aperture for the SPS and the HERA proton ring,” Part. Accel. **54**, 223–235 (1996).
- <sup>14</sup>Brüning, Oliver Sim., *An analysis of the long-term stability of the particle dynamics in hadron storage rings*, Ph.D. thesis, Hamburg Univ., Hamburg (1994), presented on May 1994.
- <sup>15</sup>Chao, A., Johnson, D., Peggs, S., Peterson, J., Saltmarsh, C., Schachinger, L., Meller, R., Siemann, R., Talman, R., Morton, P., Edwards, D., Finley, D., Gerig, R., Gelfand, N., Harrison, M., Johnson, R., Merminga, L., and Syphers, M., “Experimental Investigation of Nonlinear Dynamics in the Fermilab Tevatron,” Phys. Rev. Lett. **61**, 2752–2755 (1988).
- <sup>16</sup>Chatrchyan, S. *et al.* (CMS Collaboration), “Observation of a new boson at a mass of 125 GeV with the CMS experiment at the LHC,” Phys.Lett. **B716**, 30–61 (2012).
- <sup>17</sup>Chirikov, B. V., “A universal instability of many-dimensional oscillator systems,” Physics Report **52**, 263–379 (1979).
- <sup>18</sup>Chirikov, B. V., Ford, J., and Vivaldi, F., “Some numerical studies on Arnold diffusion in a simple model,” in *American Institute of Physics Conference Series*, American Institute of Physics Conference Series, Vol. 57 (1980) pp. 323–340.
- <sup>19</sup>Collier, P. and Schmickler, H., “Systematic studies of the LEP working point,” in *Proceedings of the 1995 Particle Accelerator Conference, Dallas, TX, USA*, CERN-SL-95-52 OP, edited by L. T. Gennari and R. H. Siemann (IEEE, 1996) pp. 554–556.
- <sup>20</sup>Cornacchia, M., “Correction of half-integer resonances at injection,” Tech. Rep. CERN-SPS-Commissioning-Report-27 (CERN, Geneva, 1976).
- <sup>21</sup>Courant, E. D., “Non-linearities in the AG synchrotron,” in *Proceedings of the CERN Symposium on High Energy Accelerators and Pion Physics, 1st International Conference on High Energy Accelerators, CERN, Geneva, Switzerland*, CERN Yellow Report, Vol. 1,



- edited by E. Regenstreif (1956) pp. 254–261.
- <sup>22</sup>Courant, E. D. and Sweet, S. H., “Theory of the alternating-gradient synchrotron,” *Annals of Physics* **3**, 1–48 (1958).
- <sup>23</sup>Dragt, A. J., “A method of transfer maps for linear and nonlinear beam elements,” in *Proceedings of the 1979 Particle Accelerator Conference, San Francisco, California, USA*, Transactions on Nuclear Science, Vol. NS-26, 3, edited by R. Hendrickson (IEEE, 1979) pp. 3601–3603.
- <sup>24</sup>Dragt, A. J., “Lectures on nonlinear orbit dynamics,” in *Proceedings of the summer school on Physics of High Energy Part. Accel.*, AIP Conference Proceedings, Vol. 87, edited by R. A. Carrigan, F. R. Huson, and M. Month (American Institute of Physics, 1982) pp. 147–313.
- <sup>25</sup>Dragt, A. J. and Finn, J. N., “Lie series and invariant functions for analytic symplectic maps,” *Journal of Mathematical Physics* **17**, 2215–2227 (1976).
- <sup>26</sup>Dumas, H. S. and Laskar, J., “Global dynamics and long-time stability in Hamiltonian systems via numerical frequency analysis,” *Phys. Rev. Lett.* **70**, 2975–2979 (1993).
- <sup>27</sup>Forest, E., *Beam dynamics: a new attitude and framework*, Physics and Technology of Particle and Photon Beams (Harwood, Sidney, 1998).
- <sup>28</sup>Forest, E., Berz, M., and Irwin, J., “Normal form methods for complicated periodic systems: A complete solution using differential algebra and lie operators,” *Part. Accel.* **24**, 91–107 (1989).
- <sup>29</sup>Franchetti, G., Franczak, B., and Schütt, P., “A benchmarking experiment in SIS for dynamic aperture induced beam loss,” GSI Text. Note , 05–10 (2004).
- <sup>30</sup>Franchetti, G., Schütt, P., Hoffmann, T., Rumolo, G., and Franchi, A., “Mapping of the resonances in SIS18,” GSI Text. Note , 02–17 (2005).
- <sup>31</sup>Giovannozzi, M., Scandale, W., and Todesco, E., “Prediction of long-term stability in large hadron colliders,” *Part. Accel.* **56**, 195–225 (1997).
- <sup>32</sup>Hagedorn, R., *Stability and amplitude ranges of two-dimensional non-linear oscillations with periodical hamiltonian applied to betatron oscillations in circular Part. Accel., part I and II* (CERN, Geneva, 1957).
- <sup>33</sup>Hagedorn, R., Hine, M. G. N., and Schoch, A., “Non-linear orbit problems in synchrotrons,” in *Proceedings of the CERN Symposium on High Energy Accelerators and Pion Physics, 1st International Conference on High Energy Accelerators, CERN, Geneva*,

- Switzerland, CERN Yellow Report, Vol. 1, edited by E. Regenstreif (1956) pp. 237–253.
- <sup>34</sup>Hagedorn, R. and Schoch, A., *Stability and amplitude ranges of two-dimensional non-linear oscillations with periodical hamiltonian applied to betatron oscillations in circular Part. Accel., part III* (CERN, Geneva, 1957).
- <sup>35</sup>Irwin, J., “Diffusive losses from SSC particle bunches due to long range beam-beam interactions,” Tech. Rep. SSC-233 (Lawrence Berkeley Laboratory, 1989).
- <sup>36</sup>Jackson, J., *Classical Electrodynamics*, 3rd ed. (John Wiley and Sons, New York, 1999).
- <sup>37</sup>Jin, L., Papaphilippou, Y., and Schmidt, F., “Improvement of lhc dynamic aperture via octupole spool pieces for the nominal tunes,” Tech. Rep. CERN-LHC-Project-Report-253 (CERN, Geneva, 1998).
- <sup>38</sup>Koutchouk, J.-P., “The LHC dynamic aperture,” in<sup>49</sup>, pp. 372–376.
- <sup>39</sup>Laskar, J., “Secular evolution of the solar system over 10 million years,” *Astronomy and Astrophysics* **198**, 341–362 (1988).
- <sup>40</sup>Laskar, J., “The chaotic motion of the solar system - A numerical estimate of the size of the chaotic zones,” *Icarus* **88**, 266–291 (1990).
- <sup>41</sup>Laskar, J., “Frequency analysis for multi-dimensional systems. Global dynamics and diffusion,” *Physica D Nonlinear Phenomena* **67**, 257–281 (1993).
- <sup>42</sup>Laskar, J., “Introduction to frequency map analysis,” in *Proceedings of NATO Advanced Study Institutes, Hamiltonian Systems with Three or More Degrees of Freedom*, Series C: Mathematical and Physical Sciences, Vol. 533, edited by C. Simó (Kluwer, 1995) pp. 134–150.
- <sup>43</sup>Laskar, J., “Frequency map analysis and part. accel.” in *Proceedings of the 2003 Particle Accelerator Conference, Portland, Oregon, USA*, WOAB001 (IEEE, 2003) pp. 378–382.
- <sup>44</sup>Laskar, J., “Frequency map analysis and quasiperiodic decompositions,” in *Proceedings of the school Hamiltonian systems and Fourier analysis: New Prospects for Gravitational Dynamics*, *Advances in Astronomy & Astrophysics*, Vol. 344, edited by D. Benest, C. Froeschlé, and E. Lega (Cambridge Scientific Publishers, 2005) pp. 130–159.
- <sup>45</sup>Laskar, J., Froeschlé, C., and Celletti, A., “The measure of chaos by the numerical analysis of the fundamental frequencies. Application to the standard mapping,” *Physica D Nonlinear Phenomena* **56**, 253–269 (1992).
- <sup>46</sup>Laskar, J. and Robin, D., “Application of frequency map analysis to the ALS,” *Part. Accel.* **54**, 183–192 (1996).

- <sup>47</sup>Laskar, J. and Robutel, P., “The chaotic obliquity of the planets,” *Nature* **361**, 608–612 (1993).
- <sup>48</sup>Liuzzo, S., Biagini, M., Raimondi, P., Papaphilippou, Y., and Demma, T., “Frequency Map Analysis for SuperB,” in *Proceedings of the 3rd International Particle Accelerator Conference, New Orleans, LA, USA*, edited by F. Zimmermann and C. Eyberger (IEEE, 2012) p. TUPPC073. 3 p.
- <sup>49</sup>Luccio, A. and MacKay, W. W., eds., *Proceedings of the 1999 Particle Accelerator Conference, New York, NY, USA* (IEEE, 1999).
- <sup>50</sup>Luo, Y., Fischer, W., Abreu, N. P., Gu, X., Pikin, A., and Robert-Demolaize, G., “Six-dimensional weak-strong simulation of head-on beam-beam compensation in the Relativistic Heavy Ion Collider,” *Phys. Rev. ST Accel. Beams* **15**, 051004 (2012).
- <sup>51</sup>von Milczewski, J., Farrelly, D., and Uzer, T., “Frequency Analysis of 3D Electronic  $1/r <$  Dynamics: Tuning between Order and Chaos,” *Phys. Rev. Lett.* **78**, 1436–1439 (1997).
- <sup>52</sup>Moser, J., “The resonance lines for the synchrotron,” in *Proceedings of the CERN Symposium on High Energy Accelerators and Pion Physics, 1st International Conference on High Energy Accelerators, CERN, Geneva, Switzerland*, CERN Yellow Report, Vol. 1, edited by E. Regenstreif (1956) pp. 290–292.
- <sup>53</sup>Nadolski, L. and Laskar, J., “Review of single particle dynamics for third generation light sources through frequency map analysis,” *Phys. Rev. ST Accel. Beams* **6**, 114801 (2003).
- <sup>54</sup>Nobelprize.org., “The nobel prize in physics 2013,” (2013), [Nobel Media AB 2013. Web. 5 Mar 2014].
- <sup>55</sup>Papaphilippou, Y., “Frequency maps of LHC models,” in<sup>49</sup>, pp. 1554–1556.
- <sup>56</sup>Papaphilippou, Y., “Correction schemes for the normal octupole and decapole errors in the lhc dipoles,” Tech. Rep. CERN-LHC-Project-Report-411 (CERN, 2000).
- <sup>57</sup>Papaphilippou, Y., “Frequency and Diffusion Maps for the SNS Ring,” in *Proceedings of the 2001 Particle Accelerator Conference, Chicago, IL, USA*, edited by Y. Cho (IEEE, 2001) pp. 462–464.
- <sup>58</sup>Papaphilippou, Y., Farvacque, L., Ropert, A., and Laskar, J., “Probing the Non Linear Dynamics of the ESRF Storage Ring with Experimental Frequency Maps,” in *Proceedings of the 2003 Particle Accelerator Conference, Portland, OR, USA*, edited by C. Horak (IEEE, 2003) pp. 3189–3191.

- <sup>59</sup>Papaphilippou, Y. and Laskar, J., “Frequency map analysis and global dynamics in a galactic potential with two degrees of freedom.” *Astronomy & Astrophysics* **307**, 427–449 (1996).
- <sup>60</sup>Papaphilippou, Y. and Laskar, J., “Global dynamics of triaxial galactic models through frequency map analysis,” *Astronomy & Astrophysics* **329**, 451–481 (1998).
- <sup>61</sup>Papaphilippou, Y. and Schmidt, F., “Normal form approaches and resonance analysis of LHC models,” in *Proceedings of the 16th Advanced ICFA beam dynamics workshop on nonlinear and collective phenomena in beam physics*, AIP Conference Proceedings, Vol. 468, edited by M. Cornacchia, J. Kono, and S. Chattopadhyay (American Institute of Physics, 1999) pp. 107–118.
- <sup>62</sup>Papaphilippou, Y., Skokos, C., Farvacque, L., Plouviez, E., Revol, J.-L., *et al.*, “Experimental Frequency Maps for the ESRF Storage Ring,” in *Proceedings of the 2004 European Particle Accelerator Conference, Lucerne, Switzerland*, edited by J. Chrin, C. Petit-Jean-Genaz, J. Poole, C. Prior, and H.-A. Synal (European Physical Society Accelerator Group, 2004) pp. 2050–2052.
- <sup>63</sup>Papaphilippou, Y. and Zimmermann, F., “Weak-strong beam-beam simulations for the Large Hadron Collider,” *Phys. Rev. ST Accel. Beams* **2**, 104001 (1999).
- <sup>64</sup>Papaphilippou, Y. and Zimmermann, F., “Estimates of diffusion due to long-range beam-beam collisions,” *Phys. Rev. ST Accel. Beams* **5**, 074001 (2002).
- <sup>65</sup>Robin, D., Steier, C., Laskar, J., and Nadolski, L., “Global Dynamics of the Advanced Light Source Revealed through Experimental Frequency Map Analysis,” *Phys. Rev. Lett.* **85**, 558–561 (2000).
- <sup>66</sup>Roncarolo, F., Arduini, G., Arimatea, C., Jacquet, D., Normann, L., and Pereira, L., “SPS Working Point Studies,” Tech. Rep. AB-Note-2006-008. CERN-AB-Note-2006-008-ABP-MD (CERN, Geneva, 2006).
- <sup>67</sup>Roszbach, J. and Schmüser, P., “Basic course on accelerator optics,” in *Proceedings of the CAS - CERN Accelerator School : 5th General Accelerator Physics Course*, CERN Yellow Report, Vol. 94-01 (1994) pp. 17–88.
- <sup>68</sup>Ruth, R., “Single Particle Dynamics in Circular Accelerators,” in *Proceedings of the USPAS-United States Particle Accelerator School: The Physics of Part. Accel.*, AIP Conference Proceedings, Vol. 153, edited by M. Month and M. Dienes (1987) pp. 150–235.

- <sup>69</sup>Schmidt, F., “Sixtrack version 1.2: single particle tracking code treating transverse motion with synchrotron oscillations in a symplectic manner; user’s reference manual,” Tech. Rep. CERN-SL-94-56 (CERN, Geneva, 1994).
- <sup>70</sup>Schmidt, F., Chiu, C. Y., Goddard, B., Jacquet, D., Kain, V., Lamont, M., Mertens, V., Uythoven, J., and Wenninger, J., “MAD-X PTC Integration,” in *Proceedings of the 2005 Particle Accelerator Conference, Knoxville, Tennessee, USA* (IEEE, 2005) pp. 1272–1274.
- <sup>71</sup>Schmidt, F., Willeke, F., and Zimmermann, F., “Comparison of methods to determine long-term stability in proton storage rings,” *Part. Accel.* **35**, 249–256 (1991).
- <sup>72</sup>Schoch, A., *Theory of linear and non-linear perturbations of betatron oscillations in alternating gradient synchrotrons*, CERN Yellow Report (CERN, Geneva, 158).
- <sup>73</sup>Sen, T. and Ellison, J. A., “Diffusion due to beam-beam interaction and fluctuating fields in hadron colliders,” *Phys. Rev. Lett.* **77**, 1051–1054 (1996).
- <sup>74</sup>Sun, C., Robin, D. S., Nishimura, H., Steier, C., and Wan, W., “Small-emittance and low-beta lattice designs and optimizations,” *Phys. Rev. ST Accel. Beams* **15**, 054001 (2012).
- <sup>75</sup>Tennyson, J. L., “Beam-Beam stability in the SSC, a preliminary report,” Tech. Rep. SSC-155 (Lawrence Berkeley Laboratory, 1988).
- <sup>76</sup>Tomas-Garcia, R., *Direct Measurement of Resonance Driving Terms in the Super Proton Synchrotron (SPS) of CERN using Beam Position Monitors*, Ph.D. thesis, Valencia U., Valencia (2003), presented on 30 Mar 2003.
- <sup>77</sup>Verdier, A., “Resonance free lattices for A.G. machines.” in<sup>49</sup>, pp. 398–400.
- <sup>78</sup>Willeke, F., “Comparison of measured and calculated dynamic aperture,” in *Proceedings of the 1995 Particle Accelerator Conference, Dallas, TX, USA*, edited by L. T. Gennari and R. H. Siemann (IEEE, 1996) pp. 2747–2751.